Article

Not peer-reviewed version

Fabrication Tolerances Impact on an ODAC Based PAM-4 Transmitter

ADEBAYO EMMANUEL ABEJIDE * , João Santos , Tanay Chattopadhyay , Francisco Rodrigues , Mario Lima , Antonio Teixeira

Posted Date: 13 May 2024

doi: 10.20944/preprints202405.0793.v1

Keywords: programmable photonics circuits; photonic integrated circuits; pulse amplitude modulation; optical digital to analog converter; fabrication tolerance; passive imbalances

 doi:10.20944/preprints202405.0793.v1

Article

Fabrication Tolerances Impact on an ODAC Based PAM-4 Transmitter

Adebayo E. Abejide [1,2,3,*], João Santos [1,2,3], Tanay Chattopadhyay [4], Francisco Rodrigues [3], Mario Lima [1,2] and António Teixeira [1,2,3]

1 Instituto de Telecomunicações, Universidade de Aveiro, 3810-193 Aveiro, Aveiro, Portugal
2 Department of Electronics, Telecommunications and Informatics (DETI), Universidade de Aveiro, 3810-193 Aveiro, Portugal
3 PICAdvanced, PCI-Creative, Science Park, Edificio Central, Ilhavo, Portugal
4 Solar Division, Bidyut Unnayan Bhaban, WBPDCL, India.
* Correspondence: adebayo@ua.pt

Abstract: Photonic integrated circuits (PIC) devices are impacted by fabrication tolerances and therefore, prior knowledge of such variation could improve the PIC fabrication process and overall yield. This paper presents a method for predicting the fabrication impacts on a telecommunication optical digital to analog converter (oDAC) based pulse amplitude modulator level four (PAM-4) transmitter. Our findings allow us to estimate the production yield in fabrication scenario using symbol error rate (SER) benchmark.

Keywords: programmable photonics circuits; photonic integrated circuits; pulse amplitude modulation; optical digital to analog converter; fabrication tolerance; passive imbalances

1. Introduction

As PIC maturity continues to increase leading to wide acceptability in industries and commercial, the complexity of PIC has also increased due to large number of components on a single chip [1,2]. Demonstrations with more than 1500 components on a single chip have been achieved and more is expected [1]. The success of PIC can be attributed to the possibility of large scale production in Silicon photonics at reduced footprint, low component-to-component losses, low power consumption and low overall packaging cost [3]. This has allowed PIC to be used in application specific photonic integrated circuits (ASPIC), which plays a role in data/tele communications, medical applications and bio sensing and even more recently in transportation such as LIDAR [4,5]. Such application specific designs require painstaking efforts, long time and high cost to achieve result and the design cannot be transformed or used for other applications except the specific purposes they are designed for [6]. In some cases, the design may fail to meet the initial objective, which implies that the process has to be repeated and the cost of production will be increased [6].

The advent of programmable photonics introduces a generic template that can be exploited to implement a variety of functionality through software [7]. Just like we have field programmable gateway arrays (FPGA) in electronics which can be reconfigured to meet specific use case of customers, programmable photonics introduce such generic functionality known as field programmable photonic gateway arrays (FPPGA) for widespread PIC design in optical communications [8]. These FPPGAs are electronically reconfigurable basic elements that allow flexible configuration of a set of passive devices in order to mime several circuits without undergoing the long-time conventional fabrication circle [6,9,10]. Most of the FPPGA architectures are based on cascaded Mach Zehnder modulator (MZM) structures in various shapes and dimensions [11,12].

In this paper, a pulse amplitude modulation four level (PAM-4) transmitter based on oDAC will be analyzed using the hexagonal FPPGA mesh developed by iPronics [9,12]. This type of transmitter is an alternative approach to replace a power hungry electrical digital to analog converter (eDAC) that is required in the conventional PAM-4 signal generation [13,14]. The oDAC devices are based on

 doi:10.20944/preprints202405.0793.v1

digital modulators and passive devices such as couplers and splitters [13]. Therefore, as a result of light-interfering nature of such devices, precision is not guaranteed due to slight deviation during fabrication which may result in performance degradation and low-yield [15,16]. The programmability and reconfigurability of the iPronics FPPGA as reported in [9,10] are applied to oDAC PAM-4 transmitter in order to investigate its potential fabrication tolerances and predict production yield, as a continuation of our work in [17].

Monte-Carlo emulation of 1000 chips to mime oDAC PAM-4 transmitter was carried out experimentally in iPronics programmable grid considering different splitter values due to fabrication errors. We then offline statistically estimated the SER performance of the devices, which we used to predict the failed and passed chips. Our aim is to demonstrate the potential of the methodology to evaluate the viability of a certain fabrication technique to meet the required yield.

2. Proposed Model

An oDAC PAM-4 transmitter is presented in Figure 1 where signal from a continuous wave (CW) laser is split into the two arms of the device through an input coupler with input coupling factor (K_{in}) and then recombined through an output coupler with output coupling factor (K_{out}). The non-return-to-zero (NRZ) electrical signals (NRZ_1 and NRZ_2) which act as most significant bit (MSB) and least significant bit (LSB) are applied to drive the modulators as shown on Figure 1.

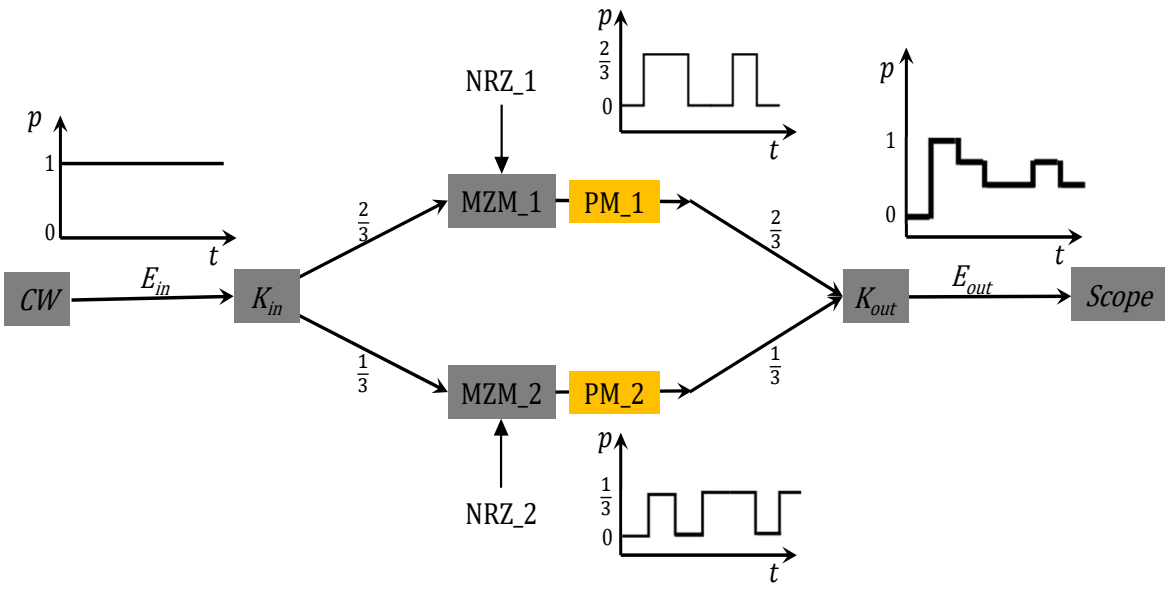

Figure 1. Structure of an oDAC PAM-4 transmitter.

Due to the sensitive nature of interferometers, imprecision in the implementation of this type of device can reduce performance during signal detection. For instance, eye diagrams at different values of K_{in} are presented in Figure 2 (a), (b) and (c). This is a challenge that requires further investigation.

 doi:10.20944/preprints202405.0793.v1

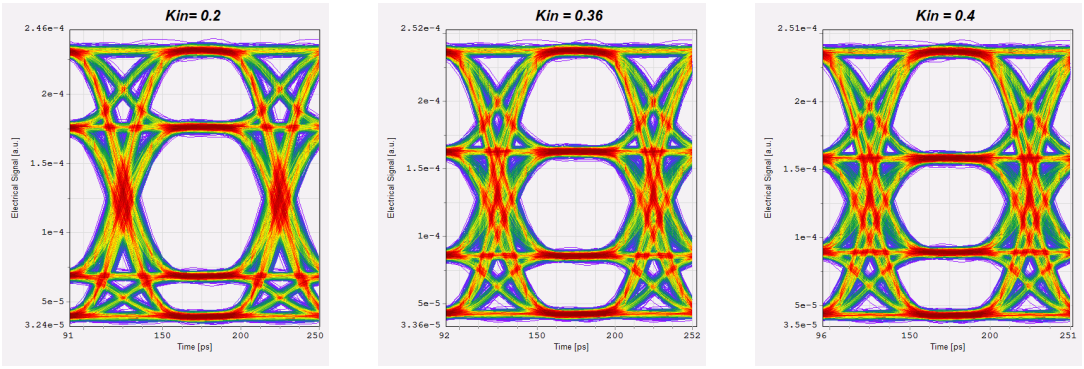

(a) (b) (c)

Figure 2. Eye diagrams of an oDAC-PAM-4 signal (a) K_{in} = 0.2 (b) K_{in} = 0.36 (c) K_{in} = 0.4.

To model this effect, one FPPGA device developed by iPronics which comprises a set of MZMs or programmable unit core (PUC)s which are hexagonally connected via replicated geometric is used. Each PUC from the arrays is itself a MZM as shown in Figure 3 which can be configured as bar state with κ = 0, cross state with κ = 1, and as tunable with κ = any value between 0 and 1.

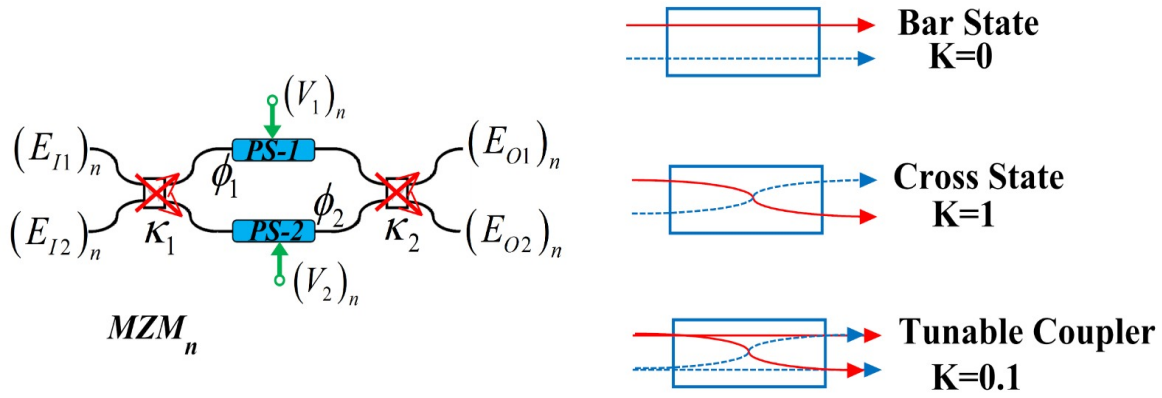

Figure 3. PUC loaded with phase shifter and heater on its both arms and its mode of implementation as Bar state, Cross state and Tunable coupler.

The mathematical expression of the output signal of a typical PUC/MZM as shown in Figure 3 (a) can be expressed as

$$\begin{bmatrix} (E_{O1})_n \\ (E_{O2})_n \end{bmatrix} = \begin{bmatrix} \sqrt{1-\kappa_2} & j\kappa_2 \\ j\kappa_2 & \sqrt{1-\kappa_2} \end{bmatrix} \times \begin{bmatrix} e^{-j\phi_1} & 0 \\ 0 & e^{-j\phi_2} \end{bmatrix} \times \begin{bmatrix} \sqrt{1-\kappa_1} & j\kappa_1 \\ j\kappa_1 & \sqrt{1-\kappa_1} \end{bmatrix} \times \begin{bmatrix} (E_{I1})_n \\ (E_{I2})_n \end{bmatrix} \tag{1}$$

where V_1 and V_2 are the applied voltages to tune the phase shifter (PS) in order to create ϕ_1 and ϕ_2 phase changes, κ_1 and κ_2, PUC input and output coupling coefficients, V_π, the half-wave voltage and $\phi_{1|2} = \frac{\pi(V_{1|2})_n}{V_\pi}$.

Hexagonal arrays of the PUCs is shown in Figure 4 (a) and it can be electrically tuned to provide functionalities such as filtering, optical interconnects and several other optical functionalities.

Preprints.org (www.preprints.org) | NOT PEER-REVIEWED | Posted: 13 May 2024 doi:10.20944/preprints202405.0793.v1

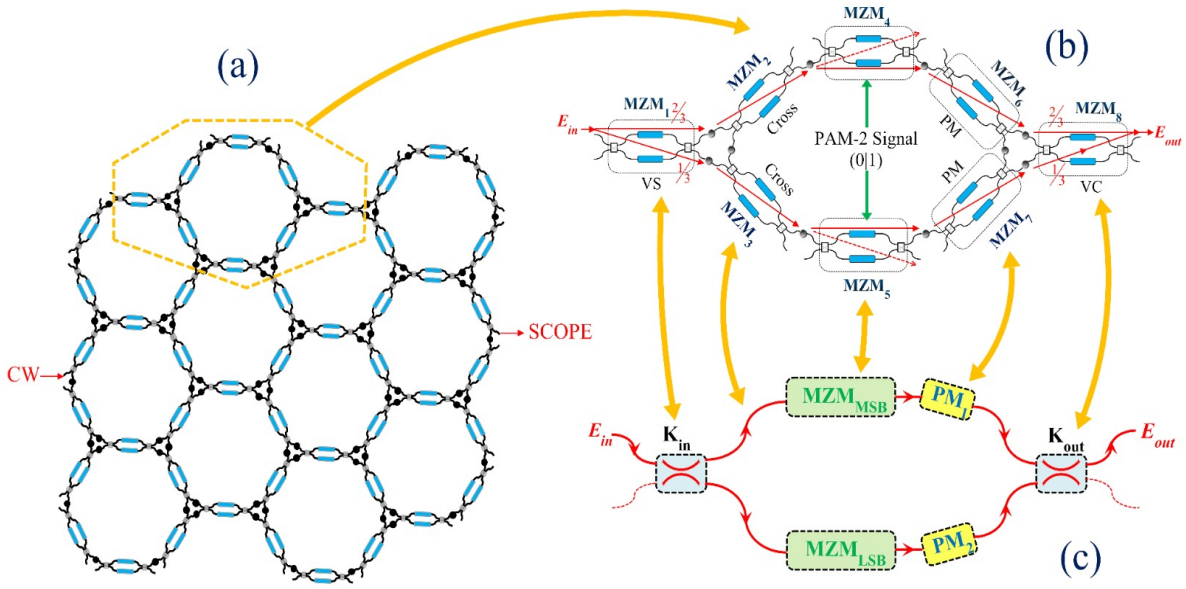

Figure 4. Building blocks of programmable photonics (a) mesh lattice with hexagonal cells, (b) and (c) oDAC-PAM-4 transmitter structure designed from the with the hexagonal cells. VS: variable splitter, PM: phase modulator, VC: variable combiner.

Furthermore, our proposed model Figure 4 (b) and (c), developed from the PUC arrays in Figure 4 (a), comprises two MZM acting as amplitude modulator (AM) (MZM_{MSB} and MZM_{LSB}) which are arranged in parallel to form the two arms just as another major MZM circuit. Light from a CW laser can then be split into the two arms of the outer MZMs via an input optical splitter (which itself is a MZM) by setting its K_{in} to 0.36 as recommended in [14].

In addition, phase modulator (PM)s mimed as PM_1 and PM_2 are placed immediately after each AM before the two signals are combined through an optical combiner with K_{out} = 0.5. By coarse adjustment of the phase of either PM_1 or PM_2, resulting in 120° phase adjustment, we can improve the PAM-4 to be equidistant.

To generate a PAM-4 signal using the proposed device, two NRZ digital signals are applied to drive the two AM where each driving implies a 1-bit modulation gate as shown on Figure 4 (b) and (c). The constellation levels of the PAM-4 signal are set to $0, 0.33, 0.66, 1$ following the oDAC design specification in [14].

Moreover, by making the input PUC (MZM_1 in Figure 4 (b)) that mimes K_{in} a random variable with Gaussian distribution, which implies that $K_{in} = K_{in} + \sigma_n$, where σ_n is the fabrication variance, we can mime the fabrication tolerance of the device. So, a Monte-Carlo emulation of the device is then carried out. For the sake of time, only 1000 devices iterations are considered. At first, the simulation is conducted for a perfect passive coupling condition with the σ_n set to 0%. Then, σ_n is further varied from 2% to 12%. As it is expected, the coupling ratio of a passive device cannot surpass 1, we opted to mime the effect of coupling resulting from the sinusoidal behaviour of MZM leading to folded "1's" and "0's".

Histogram of the Gaussian profile of the 1000 chips for a perfect passive coupler is presented in Figure 5(**a**) while histograms of increased σ_n from 2-12% are presented in Figure 5(**b**), 5(**c**) and 5(**d**) respectively. No sign of imbalance is observed on Figure 5(**a**) as expected since no error is added in this case. From the results in Figure 5(**b**), 5(**c**) and 5(**d**), L_{00} remains unchanged despite increased σ_n since this level implies an absence of light. However, increased σ_n significantly impaired L_{01} and L_{10} due to overlapping which may result in decision error. L_{11} maintains improvement when compared with L_{01} and L_{10}. This is because, L_{11} has the highest signal-to-noise ratio since the highest signal power occurred at this level. Nevertheless, impact of increased σ_n can be seen to cause L_{11} to fold back towards L_{10}.

 doi:10.20944/preprints202405.0793.v1

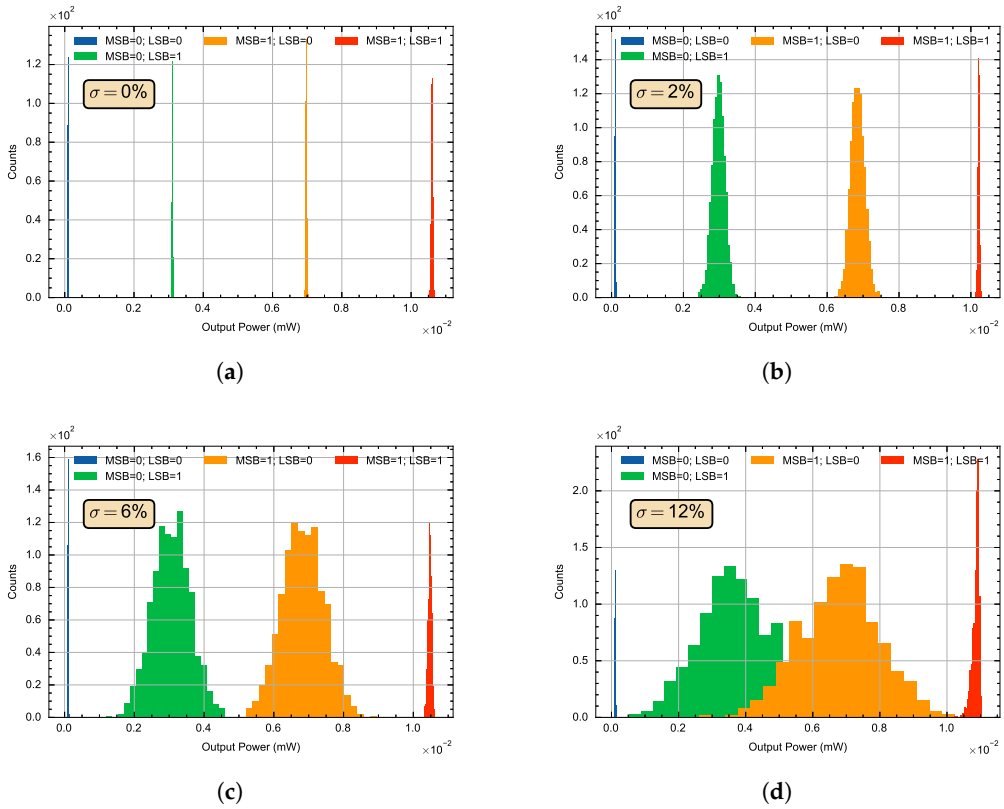

Figure 5. Histograms of the Gaussian profile of 1000 oDAC device iteration for (a) 0%, (b) 2%, (c) 6%, (d) 12%.

Next, we have optimized to ensure equidistant of amplitude levels of our PAM-4 signal. As the maximum phase shift cannot exceed 2π, the phases of both PMs (PM_1 and PM_2) are swept from 0 to 2π radians. Variation of the amplitude levels of the oDAC-PAM-4 transmitter's against phase are obtained and presented in Figure 6(**b**) and Figure 6(**a**) for PM_1 and PM_2 as in Figure 4 (c), showing the distribution of signal amplitude against phase. ER of the PAM-4 eyes against varying phase of PM_1 and PM_2 are also presented in Figure 6(**c**) and Figure 6(**d**) showing how phase variation impact the signal's extinction ratio (ER). We have set the phase of PM_2 to 2.4 radians for further analysis conducted on the oDAC-PAM-4 transmitter in this study.

Preprints.org (www.preprints.org) | NOT PEER-REVIEWED | Posted: 13 May 2024 doi:10.20944/preprints202405.0793.v1

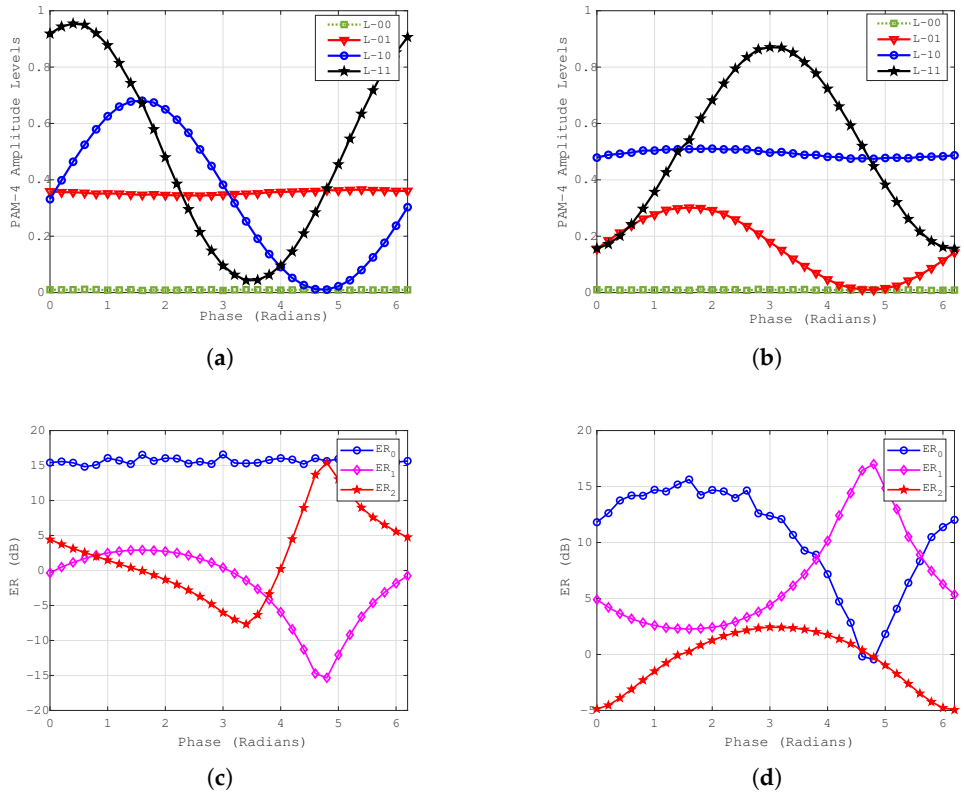

Figure 6. PAM-4 signal amplitude levels and ER against varying phase of the PMs in Figure 4 (b) when K = 0.36. (a) Amplitude levels against phase of the PM_1. (b) Amplitude levels against phase of the PM_2. (c) ER of the PAM-4 eyes against phase of PM_1. (d) ER of the PAM-4 eyes against phase of PM_2

2.1. Data Extraction and Analysis

The procedure for data extraction and analysis is presented in Figure 7. Since the machine can be controlled using software, the process in Figure 7 follows repeated iterations to mime 1000 oDAC PAM-4 transmitters. Specifically, while varying the value of σ_n in the devices, the signal levels of each of the transmitters are extracted for offline processing.

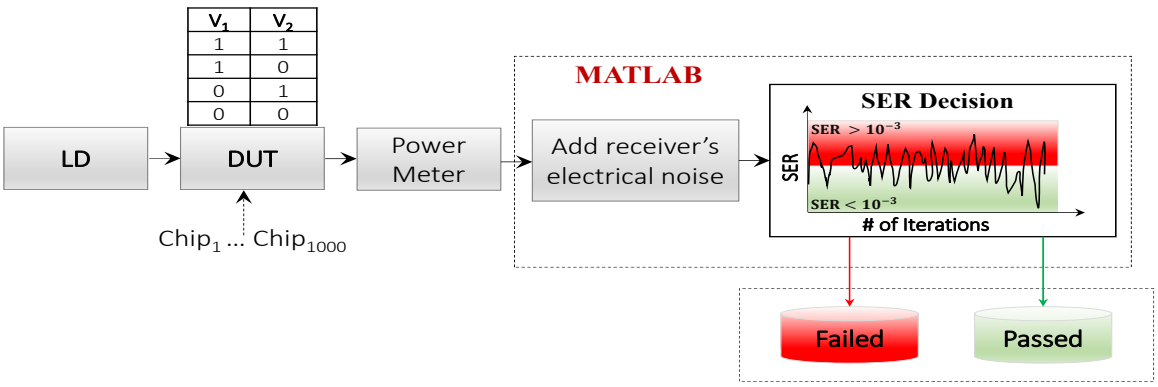

Figure 7. Procedure for data extraction from the programmable device and offline processing for error analysis.

A sketch of the decision circuit showing waveform of bits fluctuation across the four levels of the PAM-4 signal is presented in Figure A1 in Appendix A where $P(xy|ab)$ is the probability of deciding signal xy when signal ab is received and μ_i, the Gaussian pulse of the PAM-4 signal levels.

 doi:10.20944/preprints202405.0793.v1

The generalized analytical expression for estimating SER of a PAM-4 signal based on the schematic in Figure A1 is giving by Equation (A2) in Appendix B.

Therefore, solving for all the $P(I_j|I_i)$ in Figure A1 as presented in Equation (A2) using Equation (A4), we obtained Eq A5 in Appendix C.

The σ_i in Appendix B and C is the receiver's electrical noise which is estimated as the sum of thermal and short noise for a typical 10 GHz PIN receiver following the expression in [18] and it is assumed constant across the four PAM-4 levels. We have further assumed a typical detection of a 10 Gb/s signal at 1550 nm with a receiver's sensitivity of -28 dBm at SER = 10^{-3} to adjust the receiver's noise. In addition to this, the P2P power level of the signal from the machine is normalized to increase the impact of signal noise before detection. The SER bench-mark of 10^{-3} is used to determine the failed or passed chips as clearly illustrated in Figure 7.

3. Results and Discussion

The graphs of SER versus chip iteration when $\sigma_n = 0$ and when $\sigma_n = 2$ % are presented in Figure 8(**a**) and Figure 8(**b**). With light control as expected, the total 1000 iterated PIC passed the SER threshold as shown in Figure 8(**a**). When σ_n is increased to 2 %, only 3 chips out of 1000 mimed was seen to have failed while the rest passed the SER threshold we have set which implies high tolerance due to less deviation from coupling condition.

For further analysis of the results when $\sigma_n = 2$ % , PAM-4 amplitudes levels of one PIC from the failed and passed categories are extracted and simulated to obtain the PAM-4 eye diagrams of the failed and passed PIC as shown in Figure 8(**c**) and Figure 8(**d**). From the eye diagram of the failed PIC in Figure 8(**c**), it can be observed that the amplitude levels of the signal are not equidistant which resulted in error detection. Unlike the passed PIC with the eye diagram in Figure 8(**d**), an improved signal equidistant level is observed and as such, the detection is accomplished with less error at the receiver.

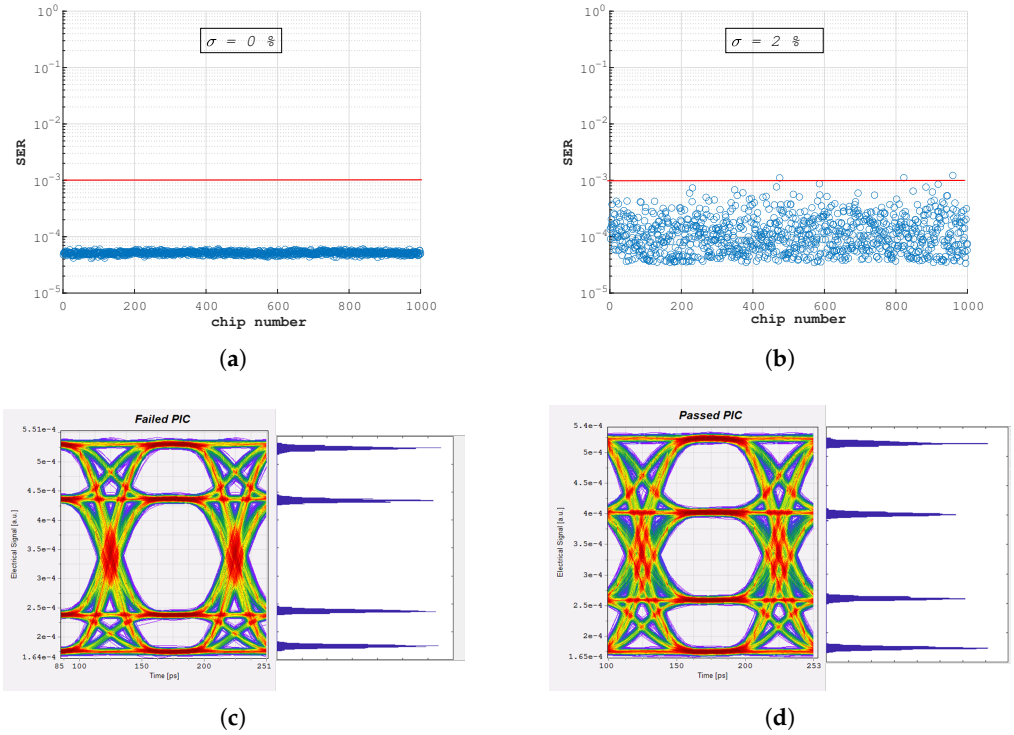

Figure 8. SER versus the number of PIC mimed at σ_n = (a) 0% (b) 2%, and eye diagram of one selected PIC from failed and passed categories when $\sigma_n = 2$ % (c) Failed PIC (d) Passed PIC.

Preprints.org (www.preprints.org) | NOT PEER-REVIEWED | Posted: 13 May 2024 doi:10.20944/preprints202405.0793.v1

Moreover, by increasing the impact of σ_n from 6 % to 12 %, it is observed that the levels 10 and 01 overlapping increases. As a result of this, the numbers of failed PICs increase, which implies low yield. Looking at the result of σ_n = 12 % in Figure 9(**b**) for instance, close to 50 % of the PIC failed due to high spread of levels 01 and 10 as clearly shown on the histogram in Figure 5(**d**), which translates to high loss in production scenario.

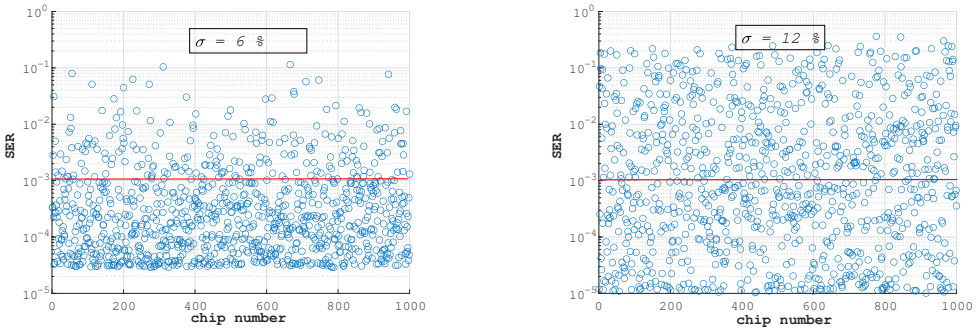

Figure 9. SER versus the number of PIC mimed at σ_n = (a) 6% (b) 12%,

In addition, the graph in Figure 10 summarizes the percentage of failed and passed chips against all instances of σ_n we have tested, which simplified our

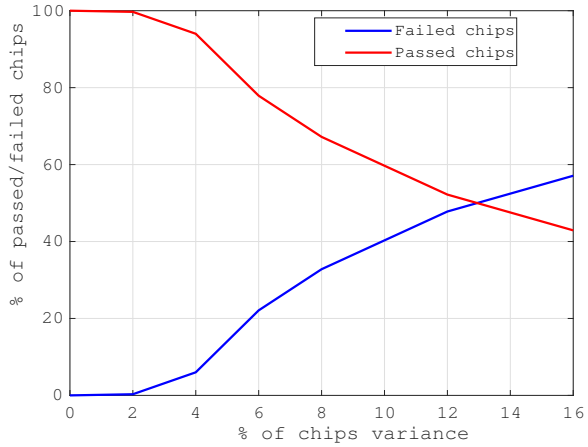

Figure 10. Percentage of failed and passed chips at different passive variances.

findings. The linear behaviour of the number of both passed and failed chips in the figure can explain what would be expected in fabrication scenario and this serve as a predictive template to analysis any passive device. Furthermore, the graph also reveals that such oDAC based PAM-4 transmitter is sensitive to component deviations resulting from variations in the passives.

4. Conclusions

In this paper, we have presented a hybrid model to study the effects of fabrication tolerance resulting from passive variation in PIC based devices. Using the flexibility of FPPGA, an oDAC-based PAM-4 telecommunication transmitter was mimed and with passive variances ranging from 0...12 % while mimicking the production of 1000 components. Monte-Carlo emulation of the device is carried out to predict the production yield at given instances of passive variation. While bench-marking the SER to 10^{-3}, the number of failed and passed PIC have been determined at every instance of passive

 doi:10.20944/preprints202405.0793.v1

variances we have tested. These findings enable robust designs which consider critically the sensitive effect of passive variability on designed components and can be formulated into new design rules .

Author Contributions: A. E A: Writing-original draft, Visualization, Conceptualization, Methodology, Investigation, A. T: Visualization, Conceptualization, Supervision, Funding Acquisition, M. L: Supervision, Review, J. S: Investigation, Software, Methodology, T.C: Review, Visualization, Methodology, Investigation F.R: Software, Review, Visualization. All authors have read and agreed to the published version of the manuscript.

Funding: This work is supported by the European Regional Development Fund (FEDER), through the Competitiveness and Internationalization Operational Program (COMPETE 2020) of the Portugal 2020 framework [Project POWER with Nr. 070365 (POCI-01-0247-FEDER- 070365)]. The work is also supported by the European Commission through the HORIZON-JU-SNS-2022 FLEX-SCALE project with Grant Agreement number 101096909.

Institutional Review Board Statement: Not applicable.

Informed Consent Statement: Not applicable.

Data Availability Statement: Not applicable.

Conflicts of Interest: The authors declare no conflict of interest.

Acronym

AM	amplitude modulator
ASPIC	application specific photonic integrated circuits
CW	continuous wave
eDAC	electrical digital to analog converter
ER	extinction ratio
FPGA	field programmable gateway arrays
FPPGA	field programmable photonic gateway arrays
K_{in}	input coupling factor
K_{out}	output coupling factor
LSB	least significant bit
NRZ	non-return-to-zero
MSB	most significant bit
MZM	Mach Zehnder modulator
oDAC	optical digital to analog converter
PAM-4	pulse amplitude modulator level four
PAM-8	pulse amplitude modulator level eight
PAM-16	pulse amplitude modulator level sixteen
PIC	Photonic integrated circuits
PUC	programmable unit cell
PM	phase modulator
PS	phase shifter
PUC	programmable unit core
QAM	quadrature amplitude modulation
SER	symbol error rate

Appendix A

Probability density of the four PAM levels are the combination of four Gaussian functions and can be written from generalized Gaussian probability density function as [19,20],

$$f(x) = \sum_{i=0}^{3} \frac{1}{\sigma_i \sqrt{2\pi}} e^{\left[-\left(\frac{|x-\mu_i|}{\sigma_i \sqrt{2}}\right)^2\right]} \tag{A1}$$

 doi:10.20944/preprints202405.0793.v1

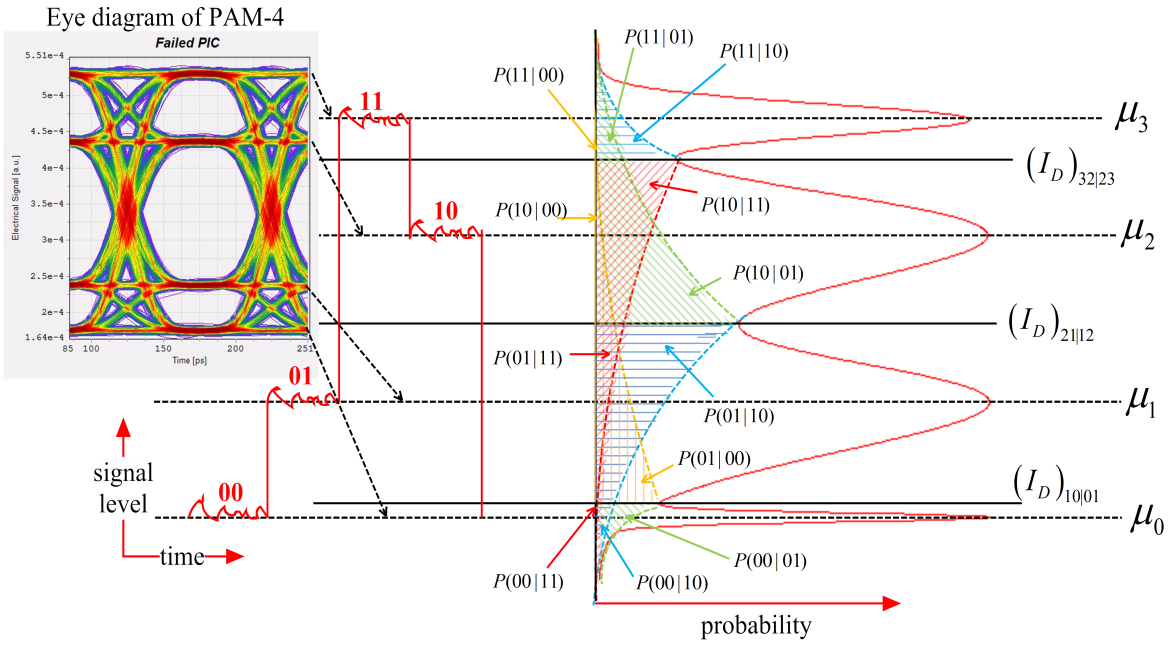

Figure A1. PAM-4 signal waveform showing the signal levels and equivalent Gaussian probability densities of the four levels. Inset is an eye diagram of a simulated 10 Gbps hybrid PAM-4 signal.

Appendix B

$$\begin{aligned} SER_{PAM-4} =& p(00)\{P(01|00)+P(10|00)+P(11|00)\}+ \\ & p(01)\{P(00|01)+P(10|01)+P(11|01)\}+ \\ & p(10)\{P(00|10)+P(01|10)+P(11|10)\}+ \\ & p(11)\{P(00|11)+P(01|11)+P(10|11)\} \end{aligned} \tag{A2}$$

This equation can be summarized as

$$SER_{PAM-4} = \sum_{i=0}^{3}\left\{ p(I_i) \times \sum_{\substack{j=0 \\ j\neq i}}^{3} P(I_j|I_i) \right\} \tag{A3}$$

where $P(I_j|I_i)$ can be expressed as

$$P(I_j|I_i) = \pm\frac{1}{2} erfc\left(\frac{\left|(I_D)_{ji|ij} - \mu_i\right|}{\sigma_i\sqrt{2}} \right) \tag{A4}$$

where μ_i and σ_i are the mean and standard deviation of i^{th} Gaussian level of the PAM-4 signal. $p(I_i) = p(00) = p(01) = p(10) = p(11) = \frac{1}{4}$ is the probability of receiving signal level I_i which is equally possible. In addition, depending on the noise contribution due to signal impairment, there is probability that signal xy will constitute an error to symbol ab across the four Gaussian pulses in Figure A1. $erfc(\cdot)$ is the complimentary error function and $(I_D)_{ji|ij}$ is the threshold values of the signal level I_i and I_j. Whenever signal detection is done above the threshold, higher logical state is considered and vice versa.

 doi:10.20944/preprints202405.0793.v1

Appendix C

$$
\begin{aligned}
P(01|00) &= \frac{1}{2}\,\mathrm{erfc}\left(\frac{(I_D)_{10|01}-\mu_0}{\sigma_0\sqrt{2}}\right)-\frac{1}{2}\,\mathrm{erfc}\left(\frac{(I_D)_{21|12}-\mu_0}{\sigma_0\sqrt{2}}\right)\\
P(10|00) &= \frac{1}{2}\,\mathrm{erfc}\left(\frac{(I_D)_{21|12}-\mu_0}{\sigma_0\sqrt{2}}\right)-\frac{1}{2}\,\mathrm{erfc}\left(\frac{(I_D)_{32|23}-\mu_0}{\sigma_0\sqrt{2}}\right)\\
P(11|00) &= \frac{1}{2}\,\mathrm{erfc}\left(\frac{(I_D)_{32|23}-\mu_0}{\sigma_0\sqrt{2}}\right)\\
P(00|01) &= \frac{1}{2}\,\mathrm{erfc}\left(\frac{\mu_1-(I_D)_{10|01}}{\sigma_1\sqrt{2}}\right)\\
P(10|01) &= \frac{1}{2}\,\mathrm{erfc}\left(\frac{(I_D)_{21|12}-\mu_1}{\sigma_1\sqrt{2}}\right)-\frac{1}{2}\,\mathrm{erfcc}\left(\frac{(I_D)_{32|23}-\mu_1}{\sigma_1\sqrt{2}}\right)\\
P(11|01) &= \frac{1}{2}\,\mathrm{erfc}\left(\frac{(I_D)_{32|23}-\mu_1}{\sigma_1\sqrt{2}}\right)\\
P(00|10) &= \frac{1}{2}\,\mathrm{erfc}\left(\frac{\mu_2-(I_D)_{10|01}}{\sigma_2\sqrt{2}}\right)\\
P(01|10) &= \frac{1}{2}\,\mathrm{erfc}\left(\frac{\mu_2-(I_D)_{21|12}}{\sigma_2\sqrt{2}}\right)-\frac{1}{2}\,\mathrm{erfc}\left(\frac{\mu_2-(I_D)_{10|01}}{\sigma_2\sqrt{2}}\right)\\
P(11|10) &= \frac{1}{2}\,\mathrm{erfc}\left(\frac{(I_D)_{32|23}-\mu_2}{\sigma_2\sqrt{2}}\right)\\
P(00|11) &= \frac{1}{2}\,\mathrm{erfc}\left(\frac{\mu_3-(I_D)_{10|01}}{\sigma_3\sqrt{2}}\right)\\
P(01|11) &= \frac{1}{2}\,\mathrm{erfc}\left(\frac{\mu_3-(I_D)_{21|12}}{\sigma_3\sqrt{2}}\right)-\frac{1}{2}\,\mathrm{erfc}\left(\frac{\mu_3-(I_D)_{10|01}}{\sigma_3\sqrt{2}}\right)\\
P(10|11) &= \frac{1}{2}\,\mathrm{erfc}\left(\frac{\mu_3-(I_D)_{32|23}}{\sigma_3\sqrt{2}}\right)-\frac{1}{2}\,\mathrm{erfc}\left(\frac{\mu_3-(I_D)_{21|12}}{\sigma_3\sqrt{2}}\right)
\end{aligned}
\tag{A5}
$$

Some of the $P(I_j|I_i)$ cancelled out in Equation (A5) and the final expression to estimate the SER of the oDAC PAM-4 is giving by

$$
\begin{aligned}
\mathrm{SER}_{PAM-4} \;=\; \frac{1}{8}\Bigg[&\,\mathrm{erfc}\left(\frac{(I_D)_{10|01}-\mu_0}{\sigma_0\sqrt{2}}\right)+\mathrm{erfc}\left(\frac{\mu_1-(I_D)_{10|01}}{\sigma_1\sqrt{2}}\right)\\
&+\mathrm{erfc}\left(\frac{(I_D)_{21|12}-\mu_1}{\sigma_1\sqrt{2}}\right)+\mathrm{erfc}\left(\frac{\mu_2-(I_D)_{21|12}}{\sigma_2\sqrt{2}}\right)\\
&+\mathrm{erfc}\left(\frac{(I_D)_{32|23}-\mu_0}{\sigma_2\sqrt{2}}\right)+\mathrm{erfc}\left(\frac{\mu_3-(I_D)_{32|23}}{\sigma_3\sqrt{2}}\right)\Bigg]
\end{aligned}
\tag{A6}
$$

References

1. Smit, M.; Williams, K.; Tol, J.v.d. 1.3 Integration of Photonics and Electronics. 2019 IEEE International Solid-State Circuits Conference - (ISSCC), 2019, pp. 29–34. doi:10.1109/ISSCC.2019.8662321.
2. Bogaerts, W.; Rahim, A. Programmable photonics: An opportunity for an accessible large-volume PIC ecosystem. *IEEE Journal of Selected Topics in Quantum Electronics* **2020**, *26*, 1–17.

3. Dai, D.; Bauters, J.; Bowers, J.E. Passive technologies for future large-scale photonic integrated circuits on silicon: polarization handling, light non-reciprocity and loss reduction. *Light: Science & Applications* **2012**, *1*, e1–e1.
4. Billah, M.R.; Blaicher, M.; Hoose, T.; Dietrich, P.I.; Marin-Palomo, P.; Lindenmann, N.; Nesic, A.; Hofmann, A.; Troppenz, U.; Moehrle, M.; others. Hybrid integration of silicon photonics circuits and InP lasers by photonic wire bonding. *Optica* **2018**, *5*, 876–883.
5. Falconi, F.; Melo, S.; Scotti, F.; Malik, M.N.; Scaffardi, M.; Porzi, C.; Ansalone, L.; Ghelfi, P.; Bogoni, A. A Combined Radar amp; Lidar System Based on Integrated Photonics in Silicon-on-Insulator. *Journal of Lightwave Technology* **2021**, *39*, 17–23. doi:10.1109/JLT.2020.3023496.
6. Bogaerts, W. Tutorial Programmable Photonics. Optical Fiber Communication Conference (OFC) 2021. Optica Publishing Group, 2021, p. Tu1K.1. doi:10.1364/OFC.2021.Tu1K.1.
7. Fang, Z. Non-volatile programmable photonics based on phase-change materials. PhD thesis, University of Washington, 2023.
8. Zhuang, L.; Roeloffzen, C.G.; Hoekman, M.; Boller, K.J.; Lowery, A.J. Programmable photonic signal processor chip for radiofrequency applications. *Optica* **2015**, *2*, 854–859.
9. Pérez-López, D.; López, A.; DasMahapatra, P.; Capmany, J. Multipurpose self-configuration of programmable photonic circuits. *Nature communications* **2020**, *11*, 6359.
10. Pérez, D.; Gasulla, I.; Crudgington, L.; Thomson, D.J.; Khokhar, A.Z.; Li, K.; Cao, W.; Mashanovich, G.Z.; Capmany, J. Multipurpose silicon photonics signal processor core. *Nature communications* **2017**, *8*, 636.
11. Steinbrecher, G.R. Programmable photonics for quantum and classical information processing. PhD thesis, Massachusetts Institute of Technology, 2019.
12. Pérez, D.; Gasulla, I.; Capmany, J.; Soref, R.A. Reconfigurable lattice mesh designs for programmable photonic processors. *Optics Express* **2016**, *24*, 12093–12106.
13. Nazarathy, M.; Tomkos, I. Accurate power-efficient format-scalable multi-parallel optical digital-to-analogue conversion. Photonics. MDPI, 2021, Vol. 8, p. 38.
14. Nazarathy, M.; Tomkos, I. Energy-efficient reconfigurable 4| 16| 64| 256-QAM transmitter based on PAM2| 4-driven optical DACs. *IEEE Photonics Technology Letters* **2022**, *34*, 1159–1162.
15. Zand, I.; Bogaerts, W. Effects of coupling and phase imperfections in programmable photonic hexagonal waveguide meshes. *Photonics Research* **2020**, *8*, 211–218.
16. Xing, Y.; Dong, J.; Khan, U.; Bogaerts, W. Capturing the effects of spatial process variations in silicon photonic circuits. *ACS Photonics* **2022**, *10*, 928–944.
17. Lopes, G.; Abejide, A.E.; Santos, J.; Rodrigues, F.; Teixeira, A. Impact of Fabrication Tolerances on the Performance of Integrated Optics. 2023 IEEE Research and Applications of Photonics in Defense Conference (RAPID), 2023, pp. 1–2. doi:10.1109/RAPID54473.2023.10264722.
18. Agrawal, G.P. *Fiber-optic communication systems*; John Wiley & Sons, 2012.
19. Jeruchim, C, M. Techniques for Estimating the Bit Error Rate in the Simulation of Digital Communication Systems. *IEEE journal of selected areas in communications* **1984**, *SAC-2*, 153–170.
20. Raza, A.; Zhong, K.; Ghafoor, S.; Iqbal, S.; Adeel, M.; Habib, S.; Butt, Fasih, U.M.; Lu, C. SER estimation method for 56 GBaud PAM-4 transmission system. *Chinease optics Letter* **2018**, *16*, 040604–1–5.